ELSEVIER

Engineering Analysis with Boundary Elements 28 (2004) 1005–1016

ENGINEERING ANALYSIS *with* BOUNDARY ELEMENTS

www.elsevier.com/locate/enganabound

Boundary element analysis of symmetrically laminated plates

S. Syngellakis*, N. Cherukunnath

School of Engineering Sciences, Computational Engineering and Design Group, University of Southampton, Southampton SO17 1BJ, United Kingdom

Received 19 December 2003; revised 17 February 2004; accepted 23 February 2004

Available online 28 March 2004

Abstract

Symmetrically laminated plates are analysed by the boundary element method. A common numerical scheme is devised for the linear, uncoupled plane stress and plate flexure problems. A generic formulation is based on adopting the stress function and the deflection as field variables in the respective problems. Their mathematical similarity allows the use of essentially the same fundamental solution and almost identical solution algorithms. The application of plane stress and flexure analyses to several benchmark problems illustrates the versatility of the formulations and the degree of accuracy achieved. In the case of flexure in particular, comparisons are made with results from earlier boundary element analyses.

Keywords: Laminated plates; Flexure; Extension; Boundary elements; Anisotropy

1. Introduction

The most cited advantage of composites is their high specific stiffness and high specific strength compared with traditional engineering materials. Structural elements made of composites can be engineered to meet the specific demands of a particular application through various design options such as the choice of reinforcement and matrix materials, the volume fractions of fibre and matrix and the fabrication method. With regard to laminates, in particular, additional options concern layer orientation, number of layers in a given direction, thickness of individual layers, type of layer and the layer stacking sequence.

The complexities in the mechanical behaviour of composite materials demanded the development of new methods for their analysis. A detailed and accurate calculation of stresses in composite components is required for design purposes. The boundary element method (BEM) has emerged, in the late seventies, as a powerful alternative to other numerical techniques for the analysis of engineering problems. Through BEM, the dimensionality of the problem reduces by one. Thus mesh generation is comparatively easy and design changes do not require a complete re-meshing. BEM is well suited for the analysis of structures with complex geometries and loadings. Good accuracy is achieved in stress concentration and infinite domain problems.

In general, numerical composite analyses can be subdivided into micro-mechanical and macro-mechanical. BEM has been applied to both. A macroscopic view has been adopted in this paper. Effective aggregate mechanical properties are entered into such an analysis with the material usually considered anisotropic. A laminate is generally subjected to lateral and membrane forces, it therefore undergoes both extensional and flexural deformation. These two modes are uncoupled and analysed separately in symmetrically laminated plates considered here.

Several direct BEM formulations for the extensional deformation of thin elastic anisotropic plates have been developed. Rizzo and Shippy [1] obtained boundary integral equations using the displacement fundamental solution of two-dimensional anisotropic elasticity and applied their formulation to orthotropic plates. Zastrow's integral equations [2] were based on stress fundamental solutions due to force singularities and displacement fundamental solutions due to edge dislocation singularities. Indirect formulations, based on an integral equation for the stresses and fictitious boundary load distributions, have been obtained for orthotropic materials and applied to problems with only traction boundary conditions [3,4]. Lee and Mal's approach [5] was based on boundary integral equations for

* Corresponding author. Tel.: +44-23-80592844; fax: +44-23-80594813.

E-mail address: ss@soton.ac.uk (S. Syngellakis).

0955-7997/$ - see front matter © 2004 Elsevier Ltd. All rights reserved.
doi:10.1016/j.enganabound.2004.02.007

displacement and traction derived from the anisotropic elasticity solution in terms of complex potentials. Wu et al. [6,7] derived boundary integral equations for the tangential derivative of the deflection using fundamental solutions in terms of complex variables.

An early attempt at an indirect BEM analysis of the corresponding anisotropic plate flexure problem [8] relied on a single fundamental solution and a number of fictitious point loads outside the plate domain. These fictitious sources are determined by requiring that the approximate solution satisfy the boundary conditions at a consistent number of discrete points. An alternative indirect formulation [9] was restricted to a particular type of orthotropy allowing the transformation of the problem to an equivalent isotropic one. A direct formulation for orthotropic plates was first proposed by Kamiya and Sawaki [10], who adopted the methodology applied earlier to the bending of isotropic plates. Shi and Bezine [11] extended that analysis to plates of general anisotropy providing expressions for all boundary integral kernels and validating their algorithm through a range of benchmark problems.

In this paper, the previously applied direct approach is extended to the complete membrane and flexural analysis of laminates. The theory is initially developed for the coupled problem but then specialised to separate in-plane and flexure direct BEM formulations. With regard to bending, certain ambiguities regarding the theoretical basis of the method are clarified. The numerical implementation uses discontinuous linear and quadratic elements, which provide higher accuracy than constant elements as well as convenient modelling of discontinuities at corner points. The form and properties of the fundamental solution is explored and particular attention is given to the evaluation of singular integrals over elements containing the source point.

The plane stress analysis is based on the choice of the stress function as the field variable. The corresponding mathematical model is almost identical to that governing flexure using the same fundamental solution. The result is a new BEM formulation for two-dimensional anisotropic media applicable to any combination of boundary conditions. Both BEM analyses are applied to a series of benchmark problems for validation purposes. Comparison of BEM predictions with results from exact or finite element analyses lead to conclusions regarding the accuracy and efficiency of the developed numerical algorithms.

2. Laminate theory

According to the classical lamination theory, the plate is assumed to be perfectly laminated consisting of an arbitrary number of discrete layers, each individual layer being homogeneous through its thickness and in a state of plane stress. The laminated plates considered here are made by stacking orthotropic layers (or plies) symmetrically arranged about the middle reference surface. Bending-stretching coupling does not arise for these symmetrically laminated plates.

The laminate is also assumed to deform according to Kirchhoff's assumptions for the bending of thin plates. According to this theory, the membrane forces $N_{\alpha\beta}$ and bending moments $M_{\alpha\beta}$ are related to the curvatures $\kappa_{\alpha\beta}$ and mid-plane strains $\varepsilon_{\alpha\beta}$ by

$$N_{\alpha\beta} = A_{\alpha\beta\gamma\delta}\varepsilon_{\gamma\delta} \tag{1}$$

$$M_{\alpha\beta} = D_{\alpha\beta\gamma\delta}\kappa_{\gamma\delta} \tag{2}$$

where $A_{\alpha\beta\gamma\delta}$ and $D_{\alpha\beta\gamma\delta}$ are, respectively, the extensional and flexural rigidities, Greek indices ranging from 1 to 2 indicate components relative to Cartesian co-ordinates x_1, x_2 (Fig. 1) and repeated indices mean summation over their range. Strain and curvatures are related to mid-plane displacements u_α and deflection w, respectively by

$$\varepsilon_{\alpha\beta} = \frac{1}{2}(u_{\alpha,\beta} + u_{\beta,\alpha}) \tag{3}$$

$$\kappa_{\alpha\beta} = -w_{,\alpha\beta} \tag{4}$$

where a comma followed by lower Greek indices indicates differentiation with respect to the corresponding co-ordinates. The membrane forces $N_{\alpha\beta}$ and bending moments $M_{\alpha\beta}$ should also satisfy the equations of equilibrium

$$N_{\alpha\beta,\beta} + f_\alpha = 0 \tag{5}$$

$$M_{\alpha\beta,\alpha\beta} + q = 0 \tag{6}$$

where f_α is the body force assumed to be derivable from a potential function Φ according to

$$f_\alpha = -\Phi_{,\alpha} \tag{7}$$

and q is the lateral pressure. Along the smooth portions of the plate boundary Γ with normal and tangent unit vectors $\mathbf{n}$ and $\mathbf{s}$, respectively, the field variables should satisfy the conditions

either

$$p_\alpha = n_\beta N_{\alpha\beta} = \tilde{p}_\alpha \text{ or } u_\alpha = \tilde{u}_\alpha \tag{8}$$

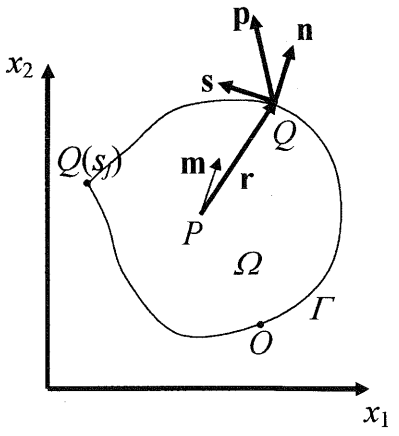

Fig. 1. Plate co-ordinates and notation.

either

$$V_n = n_\alpha M_{\alpha\beta,\beta} + \frac{\partial M_{ns}}{\partial s} = \tilde{V}_n \text{ or } w = \tilde{w} \tag{9}$$

either

$$M_n = n_\alpha n_\beta M_{\alpha\beta} = \tilde{M}_n \text{ or } \theta_n = \tilde{\theta}_n \tag{10}$$

where p_α, V_n, M_n are the in-plane boundary traction, shear force, bending moment, respectively, $\tilde{p}_\alpha, \tilde{V}_n, \tilde{M}_n$ are the corresponding pre-scribed values and M_{ns} the twisting moment

$$M_{ns} = s_\alpha n_\beta M_{\alpha\beta}$$

At any corner point j of a non-smooth boundary,

$$C_j = [\![M_{ns}]\!]_j = \tilde{C}_j \text{ or } w_j = \tilde{w}_j \tag{11}$$

where $[\![M_{ns}]\!]_j$ represents the discontinuity jump of M_{ns} at that corner.

The extensional problem described by Eqs. (1), (3), (5) and (8) can be re-formulated in terms of a stress function F such that

$$N_{\alpha\beta} = L_{\alpha\beta}F + \Phi\delta_{\alpha\beta} \tag{12}$$

where $\delta_{\alpha\beta}$ is the Kronecker delta and the operator $L_{\alpha\beta}$ defined by

$$L_{\alpha\beta} = \delta_{\alpha\beta}\nabla^2 - \frac{\partial^2}{\partial x_\alpha \partial x_\beta} \tag{13}$$

In-plane equilibrium is identically satisfied by the forces given by expressions (12), which also need to satisfy compatibility. For this purpose, $A^{-1}_{\alpha\beta\gamma\delta}$ is defined as the inverse of the extensional rigidity tensor $A_{\alpha\beta\gamma\delta}$:

$$A^{-1}_{\alpha\beta\gamma\delta}A_{\gamma\delta\lambda\mu} = \delta_{\alpha\lambda}\delta_{\beta\mu} \tag{14}$$

so that constitutive Eqs. (1) and (2) are re-formulated as

$$\varepsilon_{\alpha\beta} = A_{\alpha\beta\gamma\delta}F_{,\gamma\delta} + A^{-1}_{\alpha\beta\kappa\kappa}\Phi \tag{15}$$

$$M_{\alpha\beta} = -D_{\alpha\beta\gamma\delta}w_{,\gamma\delta} \tag{16}$$

where membrane forces and curvatures have been replaced by the stress function and deflection using Eqs. (12) and (4), respectively, and

$$\bar{A}_{\alpha\beta\gamma\delta} = A^{-1}_{\alpha\beta\kappa\kappa}\delta_{\gamma\delta} - A^{-1}_{\alpha\beta\gamma\delta}.$$

Substituting Eq. (15) into the compatibility condition

$$L_{\alpha\beta}\varepsilon_{\alpha\beta} = 0$$

and Eq. (16) into equilibrium Eq. (6) leads to the fourth-order differential equations

$$\hat{A}_{\alpha\beta\gamma\delta}F_{,\alpha\beta\gamma\delta} = -\bar{A}_{\kappa\kappa\alpha\beta}\Phi_{,\alpha\beta} \tag{17}$$

$$D_{\alpha\beta\gamma\delta}w_{,\alpha\beta\gamma\delta} = q \tag{18}$$

where

$$\hat{A}_{\alpha\beta\gamma\delta} = A^{-1}_{\kappa\kappa\lambda\lambda}\delta_{\alpha\beta}\delta_{\gamma\delta} - A^{-1}_{\alpha\beta\kappa\kappa}\delta_{\gamma\delta} - A^{-1}_{\kappa\kappa\gamma\delta}\delta_{\alpha\beta} + A^{-1}_{\alpha\beta\gamma\delta} \tag{19}$$

Omitting the body force potential from expressions (12) and referring to Fig. 1, it is possible to show that, at any point $Q(\bar{x}_1,\bar{x}_2)$ along the boundary,

$$F = \int_O^Q [(x_1 - \bar{x}_1)p_2 - (x_2 - \bar{x}_2)p_1]\mathrm{d}\Gamma \tag{20}$$

$$\frac{\partial F}{\partial n} = -s_1(Q)\int_O^Q p_1 d\Gamma - s_2(Q)\int_O^Q p_2 \mathrm{d}\Gamma \tag{21}$$

where O is an arbitrarily located origin. According to Eq. (20), F can be physically interpreted as the resultant moment about Q of the traction over OQ. Similarly, Eq. (21) describes the normal derivative of F as the component of the resultant traction over OQ in the direction $-\mathbf{s}$ at Q.

3. Integral equations

The similarity of Eqs. (17) and (18) suggests that a reciprocity relation is required for the generic linear operator

$$\Lambda_C(U) = C_{\alpha\beta\gamma\delta}U_{,\alpha\beta\gamma\delta} \tag{22}$$

where the 4th-order coefficient tensor $C_{\alpha\beta\gamma\delta}$ is considered symmetric with respect to the pair of indices $(\alpha\beta)$ and $(\gamma\delta)$. Integrating by parts, applying Green's theorem and defining the operators

$$\theta_n(U) = \frac{\partial U}{\partial n} \tag{23}$$

$$M^C_n(U) = -C_{\alpha\beta\gamma\delta}n_\alpha n_\beta U_{,\gamma\delta} \tag{24}$$

$$M^C_{ns}(U) = -C_{\alpha\beta\gamma\delta}n_\alpha s_\beta U_{,\gamma\delta} \tag{25}$$

$$V^C_n(U) = -C_{\alpha\beta\gamma\delta}n_\alpha U_{,\beta\gamma\delta} \frac{\partial M^C_{ns}}{\partial s} \tag{26}$$

it is possible to transform the identity

$$\int_\Omega C_{\alpha\beta\gamma\delta}U_{,\alpha\beta}U^*_{,\gamma\delta}\,\mathrm{d}\Omega = \int_\Omega C_{\alpha\beta\gamma\delta}U^*_{,\alpha\beta}U_{,\gamma\delta}\,\mathrm{d}\Omega \tag{27}$$

to:

$$\int_\Omega [(\Lambda_C U)U^* - (\Lambda_C U^*)U]\mathrm{d}\Omega + I^b_C(U,U^*) + J_C(U,U^*) = 0 \tag{28}$$

where U and U^* are any two functions satisfying the conditions imposed on either F or w, and

$$I^b_C(U,U^*) = \int_\Gamma [V^C_n(U)U^* - M^C_n(U)\theta_n(U^*) + M^C_n(U^*)\theta_n(U) - V^C_n(U^*)U]\mathrm{d}\Gamma \tag{29}$$

$$J_C(U,U^*) = \sum_{j=1}^{K}\left\{[\![M^C_{ns}(U)]\!]_j U^*_j - [\![M^C_{ns}(U^*)]\!]_j U_j\right\} \tag{30}$$

Ω is the plate domain bounded by contour Γ, which is smooth apart from a finite number K of corner points as shown in Fig. 1.

Boundary integral equations are derived from Eq. (28) using the fundamental solutions of $\Lambda_C(u)$ satisfying

$$C_{\alpha\beta\gamma\delta}u^*_{\lambda,\alpha\beta\gamma\delta} = \delta_\lambda(\mathbf{x}-\xi) \tag{31}$$

in an infinite domain with

$$\delta_1(\mathbf{x}-\xi) = \delta(\mathbf{x}-\xi) \tag{32}$$

$$\delta_2(\mathbf{x}-\xi) = \frac{\partial\delta(\mathbf{x}-\xi)}{\partial m(\xi)} \tag{33}$$

where δ is the Dirac delta function and m indicates an arbitrary direction specified through unit vector **m** (Fig. 1). Then, substituting u^*_λ for U^* in Eq. (28) yields

$$\int_\Omega (\Lambda_C U)u^*_\lambda \mathrm{d}\Omega - kU_\lambda(\xi) + I^b_C(U,u^*_\lambda) + JC(U,u^*_\lambda) = 0 \tag{34}$$

where $U_1 = U$ and $U_2 = \partial U/\partial m$ and k is equal to 1 or 0.5 depending on whether P is in the domain or on a smooth portion of the boundary, respectively.

Since $M^C_{ns}(U)$ appears only in the jump term (30) but not in the boundary integral (29), it may be eliminated as a boundary variable if it can be related to other boundary variables. Such a relation is derived by transforming the constitutive equations at the boundary relative to a local **n**–**s** frame of reference. Referring to Eqs. (24) and (25), this transformation needs only to be applied to $U_{,\gamma\delta}$ which becomes

$$U_{,\gamma\delta} = n_\gamma n_\delta \frac{\partial^2 U}{\partial n^2} + (n_\gamma s_\delta + s_\gamma n_\delta)\frac{\partial^2 U}{\partial n \partial s} + s_\gamma s_\delta \frac{\partial^2 U}{\partial s^2} \tag{35}$$

Substituting Eq. (35) into Eqs. (24) and (25) gives

$$M^C_n(U) = -\left(C_{nnnn}\frac{\partial U^2}{\partial n^2} + 2C_{nnns}\frac{\partial U^2}{\partial n \partial s} + C_{nnss}\frac{\partial U^2}{\partial s^2}\right) \tag{36}$$

$$M^C_{ns}(U) = -\left(C_{nsnn}\frac{\partial U^2}{\partial n^2} + 2C_{nsns}\frac{\partial U^2}{\partial n \partial s} + C_{nsss}\frac{\partial U^2}{\partial s^2}\right) \tag{37}$$

where the transformed **C**-tensor components are given by

$$\begin{aligned}
C_{nnnn} &= C_{\alpha\beta\gamma\delta}n_\alpha n_\beta n_\gamma n_\delta \\
C_{nnns} &= C_{nsnn} = C_{\alpha\beta\gamma\delta}n_\alpha n_\beta n_\gamma s_\delta \\
C_{nnss} &= C_{\alpha\beta\gamma\delta}n_\alpha n_\beta s_\gamma s_\delta \\
C_{nsns} &= C_{\alpha\beta\gamma\delta}n_\alpha s_\beta n_\gamma s_\delta \\
C_{nsss} &= C_{\alpha\beta\gamma\delta}n_\alpha s_\beta s_\gamma s_\delta
\end{aligned}$$

Eliminating $\partial^2 U/\partial n^2$ between Eqs. (36) and (37), results in:

$$M^C_{ns} = \frac{C_{nsnn}}{C_{nnnn}}M^C_n(U) - 2\left(C_{nsns} - \frac{C_{nsnn}C_{nnns}}{C_{nnnn}}\right)\frac{\partial U^2}{\partial n \partial s} - \left(C_{nsss} - \frac{C_{nsnn}C_{nnss}}{C_{nnnn}}\right)\frac{\partial U^2}{\partial s^2} \tag{38}$$

that is, an expression for M^C_{ns} in terms of

$$M^C_n,\ \frac{\partial}{\partial s}\left(\frac{\partial U}{\partial n}\right)$$

and $\partial^2 U/\partial s^2$.

4. Fundamental solutions

Explicit expressions for the first fundamental solution of Eq. (31) can be found in earlier BEM anisotropic plate analyses by Wu and Altiero [8] as well as Shi and Bezine [11], who cited relevant original work by Polish authors (in Polish). A compact form of this solution can be obtained applying Fourier transforms to Eq. (31) or, even more directly, from John's general solution for a linear elliptic equation with analytic coefficients [12]. Either of the two procedures requires complex function integration by the method of residues and finally gives

$$u^*_1 = \frac{1}{4\pi C_{2222}}\mathrm{Re}\left(\sum_{\kappa=1}^{2}\frac{\nu^2_\kappa}{\beta_\kappa}\ln\nu_\kappa\right) \tag{39}$$

where

$$\begin{aligned}
\nu_\kappa &= x_1 - \xi_1 + \lambda_\kappa(x_2 - \xi_2) \\
\beta_1 &= e_1(\lambda_1 - \lambda_2)(\lambda_1 - \bar{\lambda}_2) \\
\beta_2 &= e_2(\lambda_1 - \lambda_2)(\bar{\lambda}_1 - \lambda_2)
\end{aligned}$$

and

$$\begin{aligned}
\lambda_\kappa &= d_\kappa + \mathrm{i}e_\kappa, \\
\bar{\lambda}_\kappa &= d_\kappa - \mathrm{i}e_\kappa
\end{aligned}$$

($\kappa = 1,2; e_\kappa > 0$), are the complex roots of the 4th-order polynomial $f(\lambda)$ in $\lambda = \zeta_2/\zeta_1$ defined by

$$C_{\alpha\beta\gamma\delta}\zeta_\alpha\zeta_\beta\zeta_\gamma\zeta_\delta = C_{2222}\zeta_1{}^4 f(\lambda) \tag{40}$$

It can be shown that the second fundamental solution is given by

$$u^*_2 = \frac{\partial u^*_1(\mathbf{x}-\xi)}{\partial m(\xi)} = \frac{1}{4\pi C_{2222}}\mathrm{Re}\left[\sum_{\kappa=1}^{2}\frac{\nu_\kappa}{\beta_\kappa}(2\ln\nu_\kappa + 1)(m_1 + \lambda_\kappa m_2)\right] \tag{41}$$

Compact expressions of all other kernels appearing in integral Eq. (34) are given in the Appendix.

5. Flexure

Integral Eq. (34) is first applied to the plate flexure problem by replacing function U with deflection w and tensor $C_{\alpha\beta\gamma\delta}$ with the flexural rigidities $D_{\alpha\beta\gamma\delta}$. Also

accounting for Eq. (18) results in the boundary integral equation

$$\int_{\Omega} qw^*_{\lambda \mathrm{d}}\Omega - kw_\lambda(\xi) + I^b_D(w, w^*_\lambda) + J_D(w, w^*_\lambda) = 0 \qquad (42)$$

with the fundamental solutions still given by Eqs. (39) and (41) but represented here by w^*_λ. These solutions are interpreted as deflections of an infinite plate due to unit force and unit moment acting in the plane $m - x_3$ at the source point P. The operators defined through Eqs. (23)–(26), applied to deflection, generate expressions for the normal slope $\theta_n(w)$, bending moment $M^D_n(w)$, twisting moment $M^D_{ns}(w)$ and shear force $V^D_n(w)$ along the boundary.

The bending moments at any point within the domain are computed using the constitutive Eq. (16) with the curvatures obtained by differentiating twice the boundary integral Eq. (42) for $k = 1$ and $\lambda = 1$:

$$w_{,\alpha\beta}(\xi) = \int_{\Omega} qw^*_{1,\alpha\beta}\,\mathrm{d}\Omega + I^b_D(w, w^*_{1,\alpha\beta}) + J_D(w, w^*_{1,\alpha\beta}) \qquad (43)$$

These second partial derivatives are directly evaluated since they depend on known or already determined variables along the boundary.

6. Extension

Due to the similarity of Eq. (17) to Eq. (18), the boundary integral Eq. (34) can also be applied to the extensional problem for the stress function with the function $q'(\Phi) = -\bar{A}_{\kappa\kappa\alpha\beta}\Phi_{,\alpha\beta}$ replacing lateral pressure. In this application, U is replaced by F, u^*_λ by F^*_λ and $C_{\alpha\beta\gamma\delta}$ by $\hat{A}_{\alpha\beta\gamma\delta}$, giving the boundary integral equation

$$\int_{\Omega} q'F^*_\lambda \mathrm{d}\Omega - kF_\lambda(\xi) + I^b_A(F, F^*_\lambda) + J_A(F, F^*_\lambda) = 0 \qquad (44)$$

subject to boundary values for F and $\partial F/\partial n$ satisfying Eqs. (20) and (21) respectively.

The singular fundamental solutions F^*_λ, given by Eqs. (39) and (41), are identical in form to those for the bending problem but their physical interpretation is of course different since they are due to unit point and dipole potential sources. The interpretation of expressions $M^A_n(F), M^A_{ns}(F)$ and $V^A_n(F)$, obtained by applying the operators defined by Eqs. (24)–(26) to F, is not immediately obvious. However, using constitutive Eq. (15) and ignoring body forces, it is possible to show that, for a piece-wise rectilinear boundary, they are related to boundary strain and displacement by

$$M^A_n(F) = -\varepsilon_s = -\frac{\partial u_s}{\partial s} \qquad (45)$$

$$M^A_{ns}(F) = \varepsilon_{ns} \qquad (46)$$

$$V^A_n(F) = -\frac{\partial \varepsilon_s}{\partial n} + 2\frac{\partial \varepsilon_{ns}}{\partial s} = \frac{\partial^2 u_n}{\partial s^2} \qquad (47)$$

therefore the jump term $J_A(F, F^*_\lambda)$, obtained from Eq. (30), depends in this case on the discontinuities of shear strain (46) at the corners.

Provided that all the unknown boundary variables have been determined, the membrane stresses at any point within the domain are then computed by differentiating twice the boundary integral equation for the stress function, that is, Eq. (44) applied with $k = \lambda = 1$, with respect to the source point co-ordinates. These second-order partial derivatives are then substituted into Eq. (12).

7. Boundary element modelling

7.1. Interpolation models

The boundary integral $I^b_C(U, U^*)$, defined by Eq (29), depends on variables, which may not have been specified over part or the whole of the boundary Γ. Discontinuous models have been adopted in the present analysis to represent these unknown boundary variables. Such models not only approximate more accurately the variation of a variable over a boundary element, but also facilitate the modelling of corner discontinuities. Linear and quadratic discontinuous boundary element models have been fully described in an earlier buckling analysis of isotropic plates [13].

If the boundary unknowns are represented by $Z^{(m)}$ where $Z^{(1)} = U, Z^{(2)} = \theta_n(U), Z^{(3)} = M^C_n(U)$, and $Z^{(4)} = V^C_n(U)$, their approximation over an element would be

$$Z^{(m)} = \sum_{k=1}^{P} Z^{(m)}_k \phi_k \qquad (48)$$

where ϕ_k are the interpolation functions and P is the order of approximation, that is $P = 0$, 1, or 2 for constant, linear or quadratic elements, respectively. Then a typical boundary integral over an individual element Γ_e has the form

$$I^e_\lambda = \sum_{k=1}^{P} Z^{(m)}_k \int_{\Gamma_e} G^{(m)}_\lambda \phi_k \mathrm{d}\Gamma \qquad (49)$$

where $G^{(m)}_\lambda (\lambda = 1, 2)$ would be the fundamental solution kernel paired with variable $Z^{(m)}$ in any of integral Eqs. (34), (42) or (44).

7.2. Principal values of singular integrals

The integration in Eq. (49) over elements, which do not contain the source point is performed numerically using Gaussian quadrature. Analytical integration is however possible and indeed essential over elements containing the source point not only for achieving better accuracy but also for avoiding alternative numerical schemes to cope with

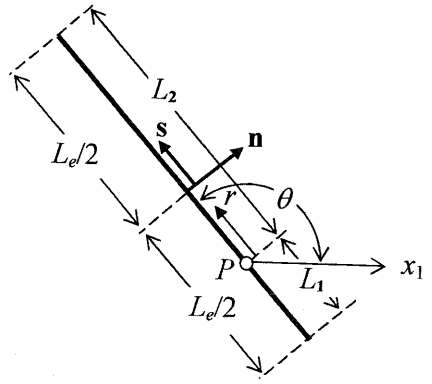

Fig. 2. Integration over boundary element containing the source point.

the r^{-1} and r^{-2} singularities of certain kernels. A local co-ordinate s, with origin at an internal node specified as the source point, is defined as shown in Fig. 2. Then the interpolation functions are expressed in terms of s so that the coefficients of $Z_k^{(m)}$ are obtained as linear combinations of

$$I_{\lambda q}^{e} = \int_{\Gamma_e} G_{\lambda}^{(m)} s^q \mathrm{d}_s \tag{50}$$

where $q = 0, \cdots, P$.

It is evident from Fig. 2 that, over a straight boundary element containing the source point,

$$v_\kappa = r(s_1 + \lambda_\kappa s_2)$$

where

$$r = \sqrt{(x_1 - \xi_1)^2 + (x_2 - \xi_2)^2}$$

Referring to the complete expressions of the various kernels $G_{\lambda}^{(m)}$ given in the Appendix, it is easily shown that, in this case, they reduce to the form

$$G_{\lambda}^{(m)}(r, \theta) = [f_{\lambda}^{(m)}(\theta) \ln r + g_{\lambda}^{(m)}(\theta)] r^{m-\lambda-1}$$

for $m-\lambda \geq 1$, or simply

$$G_{\lambda}^{(m)} = r^{m-\lambda-1} f_{\lambda}^{(m)}(\theta)$$

for $m-\lambda < 1$ since vectors $\mathbf{m} = \mathbf{n}$ and $\mathbf{s}$ all depend on the single angle θ, which is constant over that element. Hence, analytical expressions for all $I_{\lambda q}^{e}$ can be obtained by performing the integration with respect to r so that Eq. (50) is simplified to

$$I_{\lambda q}^{e} = \int_0^{L_2} G_{\lambda}^{(m)}(r, \theta) r^q \mathrm{d}r + \int_0^{L_1} G_{\lambda}^{(m)}(r, \theta + \pi)(-r)^q \mathrm{d}r$$

It should be noted that the derived expressions represent the principal values of integrals (50) only when singular integrals arise, that is, in the cases of kernels $G_1^{(1)}$ and $G_2^{(2)}$ with $q = 0$ as well as kernel $G_2^{(1)}$ with $q = 0, 1$.

7.3. Modelling of the jump term

The modelling of the jump term at corners can be based on Eq. (38), which provides a relation between M_{ns}^{C} and other boundary variables or their path derivatives. Using the adopted boundary element models, an approximation can thus be deduced for the twisting moment appearing in the jump term over the boundary elements adjacent and on either side of a corner in terms of the nodal unknowns within these elements. Since Eq. (38) involves the second derivative of a boundary variable (deflection or stress function), only the quadratic element is directly applicable in the most general case. In the case of constant or linear elements, the approximation scheme for the jump term would have to be extended to additional elements on either side of a corner.

7.4. Matrix equations

Performing the integrations with the adopted boundary element modelling transforms the boundary integral equations into a system of algebraic equations

$$\sum_{m=1}^{4} \mathbf{E}_m^C \mathbf{Z}^{(m)} = \mathbf{Q}^C \tag{51}$$

where superscript C can be either D or A depending on the problem being flexure of plane stress, respectively The coefficient matrix $\mathbf{E}_m^C$ is due to boundary integrals associated with boundary variable $Z^{(m)}$ incorporating any contribution from the jump term. Vector Q^C is due to domain integrals depending on the external action, that is, lateral pressure if $C = D$ or body forces if $C = A$. Accounting for the boundary conditions and re-arranging Eqs. (51) gives the final system of equations

$$\mathbf{H}^C \mathbf{Z} = \mathbf{P}^C \tag{52}$$

which can be solved for the vector of the boundary unknowns $\mathbf{Z}$. Since there are two independent unknowns per node, the size of the problem will be $N_b = 2N_n$ where $N_n = n_a N_e$ is the number of nodes and N_e the number of discontinuous boundary elements.

With all boundary variables known, the deflection $w$at an arbitrary point inside the domain can be computed from Eq. (42) with $k = \lambda = 1$. The plate curvatures can also be computed at any point within the plate domain from the set of boundary integral Eq. (43). These integral equations contain higher-order derivatives of the kernels but no singularity arises since the source point is always in the domain. The bending moments are finally obtained by substituting the values of the curvatures into Eq. (2).

7.5. Mixed extensional boundary value problem

If the displacement is specified along part of the boundary, then Eqs (45) and (47) imply that $M_n^A(F)$ and $V_n^A(F)$ are known, while F and $\partial F/\partial n$ cannot be determined from Eqs. (20) and (21) since they depend on partly unknown tractions. A boundary element solution of integral Eq. (44) is still however possible if BEM modelling is

applied to tractions rather than to F and $\partial F/\partial n$. Then Eqs. (20) and (21) can be transformed to matrix equations of the form

$$\mathbf{Z}^{(m)} = \mathbf{K}^{(m)}\mathbf{P};\ m = 1,2$$

where $\mathbf{P}$ is the one-dimensional array of all known and unknown tractions. Eq. (51) can then be written as

$$\left(\sum_{m=1}^{2} \mathbf{E}_m^A \mathbf{K}^{(m)}\right)\mathbf{P} + \sum_{m=3}^{4} \mathbf{E}_m^A \mathbf{Z}^{(m)} = \mathbf{Q}^C \tag{53}$$

which can be re-arranged after the application of the boundary conditions to yield any combination of unknown variables among p_1, p_2, $Z^{(3)} = M_n^A(F)$ and $Z^{(4)} = V_n^A(F)$ along the boundary.

8. Numerical results

8.1. Flexure

BEM was originally applied to a circular clamped orthotropic plate under uniform lateral pressure by Kamiya and Sawaki [10] who obtained deflection and boundary moment distributions in good agreement with Timoshenko's exact solution [14] Further results are presented here to confirm the accuracy of the BEM solution in connection with the chosen elements. The computer code implementing the analysis was written in C. The calculations were based on an orthotropic composite plate with flexural rigidities $D_{1111} = 17.337 \times 10^3$ Nm, $D_{2222} = 1.1558 \times 10^3$ Nm, $D_{1212} = 0.34675 \times 10^3$ Nm, $D_{1122} = 0.050458 \times 10^3$ Nm and thickness $h = 0.1a$ where a is the radius of the plate.

The performance of straight and curvilinear (circular arc) elements can be compared by referring to Fig. 3 showing the variation of the dimensionless edge shear force v_n defined by

$$v_n = \frac{V_n}{pa}$$

where p is the lateral pressure. It is noted in Fig. 3 that the straight element nodal values oscillate about the exact solution although the mid-element value appears to be accurate. This is probably due to ignoring the jump term at the artificially generated corner points. This oscillation almost disappears with the use of curvilinear elements, which restore boundary smoothness. It is noted that the accuracy of the results is maintained with fewer elements. This is confirmed by the domain bending moment results of Fig. 4, which shows the internal variation of the dimensionless bending moment

$$m_{11} = \frac{M_{11}}{pa^2}$$

along both axes of symmetry. Excellent agreement with the exact solution is achieved with a relatively small number of boundary elements.

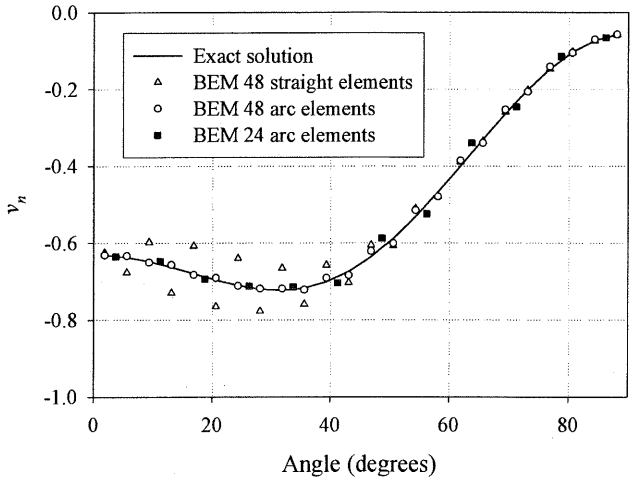

Fig. 3. Dimensionless edge shear force for a clamped circular orthotropic plate under uniform lateral pressure.

Previous results [11], based on constant boundary elements, for square orthotropic plates under various support and loading conditions were found in good agreement with the respective exact solutions [14,15]. The same high degree of accuracy was generally observed in the present BEM results obtained using both linear and quadratic discontinuous boundary elements. The calculations were based on the same material constants as those used for the circular plates. The results were further validated by comparing them with output from ANSYS [16], a general-purpose finite element package. This is essential when the available exact solution does not provide unique, stable results as happens in the case of the edge shear force in a simply supported plate due to a central point load P. Predictions of the dimensionless shear force

$$v_n = \frac{V_n a}{P}$$

based on the exact solution, ANSYS and the present BEM formulation are shown in Fig. 5. The exact solution is

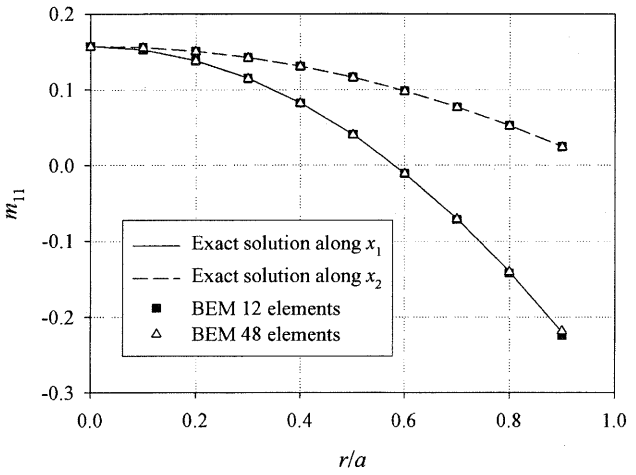

Fig. 4. Radial variation of the dimensionless bending moment m_{11} in a clamped circular orthotropic plate under uniform lateral pressure.

a series Navier solution, which fails to converge to a single value near and at the middle of the edge. It is also worth noting that the use of 8-node quadrilateral finite elements leads to a widely oscillatory solution about the correct one. It was thus necessary to use 4-node quadrilateral FE in order to establish the reliability of the BEM results.

Another interesting case, previously analysed but not validated [11], is that of a cantilever plate, clamped along the edge $x_1 = 0$ and all other edges free under a central point load. Since there is no exact solution to this problem, the boundary element predictions for the deflection were compared with those from ANSYS. The material properties adopted in the calculations were the same as those used in the previous examples. The dimensionless deflection

$$\bar{w} = \frac{D_{2222} w}{Pa^2}$$

was obtained along various key plate sections and plotted in Fig. 6. BEM and FEM predictions are seen to be very close with their agreement improving as the modelling by both methods becomes more refined.

In the previous examples involving orthotropic plates, the bending-twisting coupling stiffness terms D_{1112} and D_{2212} vanish. Such plates are special cases of general laminated plates and occur only when laminates are constructed of orthotropic or isotropic plies with principal material axes parallel to the plate axis. As a more general example, symmetrically laminated plates made up of orthotropic layers with the principal material axes not parallel to the plate axes are considered. Such laminates are characterised by the non-vanishing bending-twisting coupling stiffness terms D_{1112} and D_{2212}. Rectangular anisotropic plates with clamped edges under a uniform load were analysed. General anisotropy is simulated by assuming the plates composed of a single layer of the same orthotropic material characterised by $E_L/E_T = 10, G_{LT} = 0.25$ and

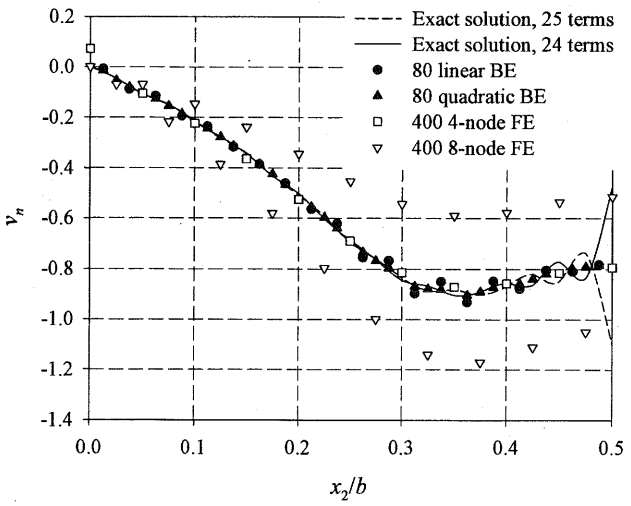

Fig. 5. Dimensionless shear force along edge $x_1 = 0$ of a simply supported square plate under central point load.

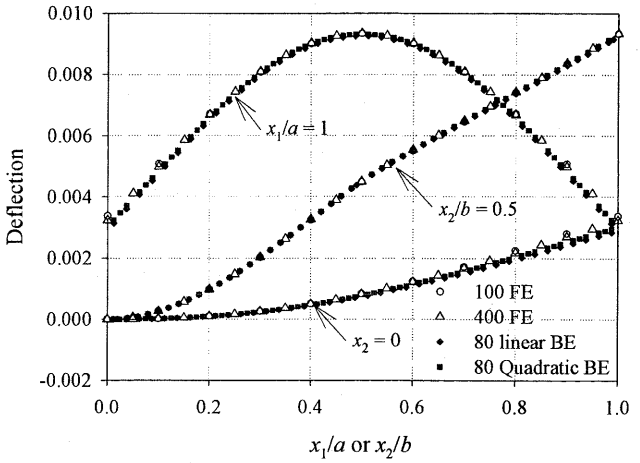

Fig. 6. Dimensionless deflection of a cantilever square plate under central point load.

$\nu_{LT} = 0.3$, but with the longitudinal material axis at various angles with the plate x-axis. Boundary element and analytical solutions [17] for the dimensionless maximum deflection defined by

$$\bar{w} = D_{1111} \frac{w_{\max}}{pb^4}$$

are listed and compared in Table 1 for various orientation of the principal orthotropic axis of the material with respect to the plate edges.

It should be noted that, for isotropic materials, the polynomial $f(\lambda)$, defined through Eq. (40) reduces to $(\lambda^2 + 1)^2$ which has double roots $\lambda = \lambda_1 = \lambda_2 = \mathrm{i}$. The form of the fundamental solution (39) is not therefore appropriate since in this case, it does not yield finite values. It was thus considered necessary to test the effectiveness and stability of the computer code for almost isotropic materials, that is, materials with properties very close to isotropic. The code proved to be robust in this seemingly unstable case. Moreover, results obtained for square simply supported plates were found in excellent agreement with the respective isotropic solutions.

Table 1
Maximum dimensionless deflection ($\bar{w} \times 10^3$) of clamped rectangular anisotropic plates under uniform lateral pressure

Reinforcement orientation (deg)	$a/b = 1$		$a/b = 2$	
	Analysis [17]	BEM	Analysis [17]	BEM
0	2.72	2.713	18.9	18.95
15	2.96	2.957	1.74	17.45
30	3.52	3.521	13.6	13.14
45	3.83	3.833	7.89	7.88
60	3.52	3.52	4.49	4.41
75	2.96	2.957	3.10	2.97
90	2.72	2.713	2.75	2.61

8.2. Extension

Initially the membrane stress analysis was tested on simple benchmark problems involving uniform stress states Using linear boundary elements, the results were not as accurate as expected. This was due to modelling the known boundary variation of F as linear while, in fact, it was quadratic. The error in the determination of boundary variables affected the accuracy of domain membrane stresses. The implementation of quadratic elements improved the accuracy of solution considerably. Using these elements, the determined values of boundary variables $M_n^A(F)$ and $V_n^A(F)$ were shown to satisfy exactly Eqs. (45) and (47).

The analysis was validated further by applying it to a series of two-dimensional problems as shown in Fig. 7. The laminated plates were assumed orthotropic with the following extensional stiffness coefficients:

$$A_{1111} = 1.8181 \times 10^9 \text{ N/m}$$
$$A_{2222} = 1.0346 \times 10^8 \text{ N/m}$$
$$A_{1122} = 2.8969 \times 10^7 \text{ N/m}$$
$$A_{1212} = 7.17 \times 10^7 \text{ N/m}$$

The corresponding compliances $\hat{A}_{\alpha\beta\gamma\delta}$, replacing $C_{\alpha\beta\gamma\delta}$ in the fundamental solution (39), are:

$$\hat{A}_{1111} = 9.7089 \times 10^{-9} \text{ m/N}$$
$$\hat{A}_{2222} = 0.55249 \times 10^{-9} \text{ m/N}$$
$$\hat{A}_{1122} = -0.1547 \times 10^{-9} \text{ m/N}$$
$$\hat{A}_{1212} = 3.48675 \times 10^{-9} \text{ m/N}$$

The presented results were obtained using quadratic elements and a computer code written in C.

The plate in Fig. 7(a) is under uniform in-plane pressure, partially and symmetrically applied to the edges, so that the membrane stress distribution inside the plate domain is not uniform. The boundary was divided into a total of 80 elements (20 along each side). The dimensions a and b were both taken equal to 1 m and pressures $p_1 = p_2 = 1$ MPa were applied on the edges over lengths $c = d = 0.5$m. The same plate was analysed using ANSYS adopting a regular mesh of 400 8-node quadrilateral elements (PLANE82). The results from both analyses for the variation of N_{11} and N_{22} along the centrelines parallel to the x_1 and the x_2 axis are shown in Figs. 8 and 9. Excellent agreement between the two solutions is noted, the difference between them being much less than 1% at most points.

The plate in Fig. 7(b) was subjected to symmetrically positioned, point in-plane forces acting at the middle of each edge. This is a case of highly non-uniform membrane stress distribution inside the plate domain. A point load of $P_1 = P_2 = 1$ MN was applied on the edges, while the adopted geometry as well as BEM and FEM modelling were identical to those for the previous

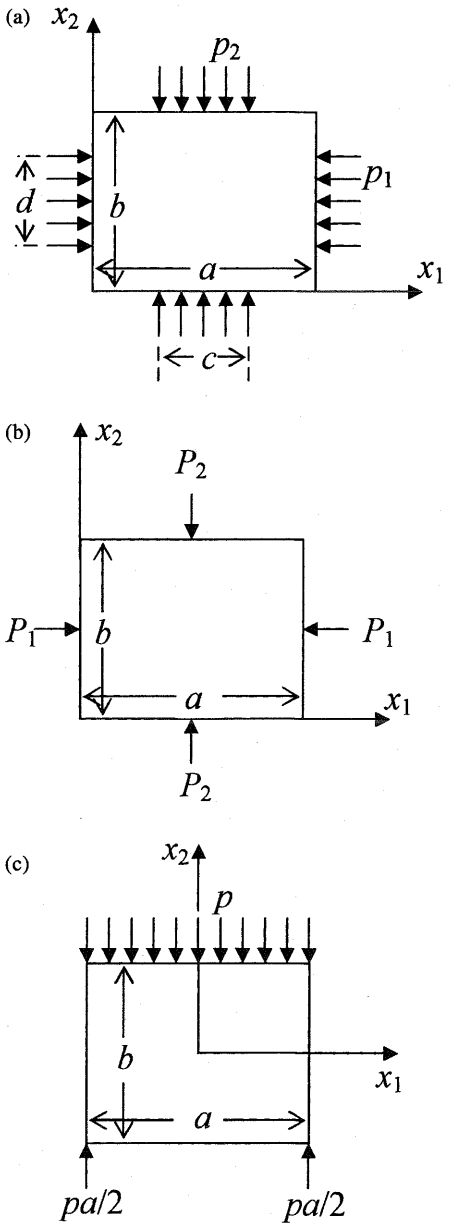

Fig. 7. Analysed examples of membrane stress states.

problem. The results from both analyses for the variation of N_{11} and N_{22} along the centrelines parallel to the x_1 and the x_2 axis are shown in Figs. 10 and 11. The agreement between the two predictions is again excellent away from the points of application of the point loads where the stresses are singular. It is worth noting that the BEM results appear to be more stable and reliable than the corresponding FEM ones as the solution approaches these singular points.

The plate in Fig. 7(c) can be considered as a flat, narrow-section, simply-supported beam undergoing bending under the action of uniform lateral load on its top surface. The adopted dimension and loading were $a = 5$m, $b = 1$ m and $p = 1$MN/m. The boundary was divided into a total

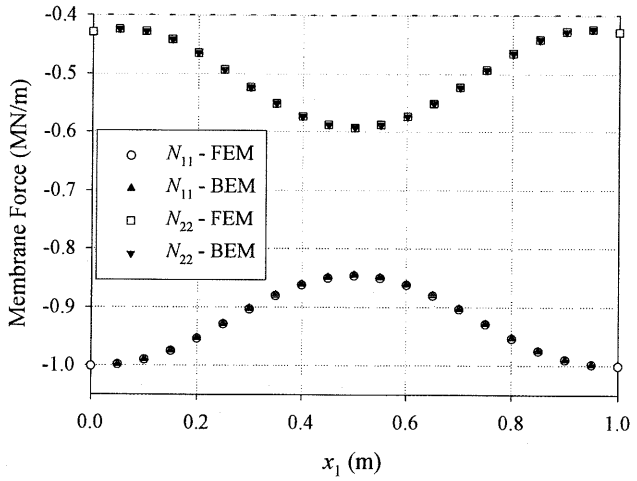

Fig. 8. Membrane forces along the centreline parallel to x_1 axis for the problem of Fig. 7(a).

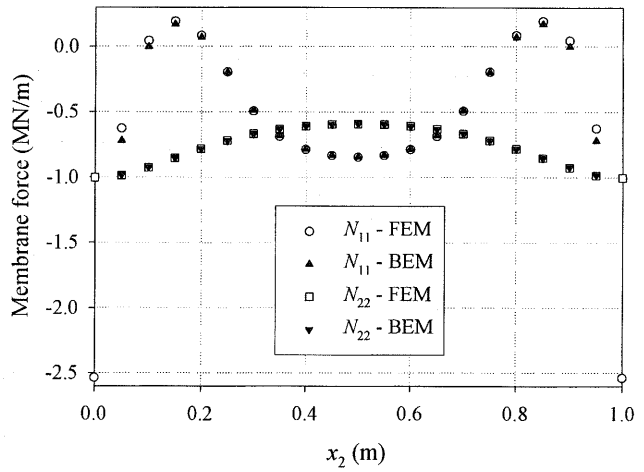

Fig. 9. Membrane forces along the centreline parallel to x_2 axis for the problem of Fig. 7(a).

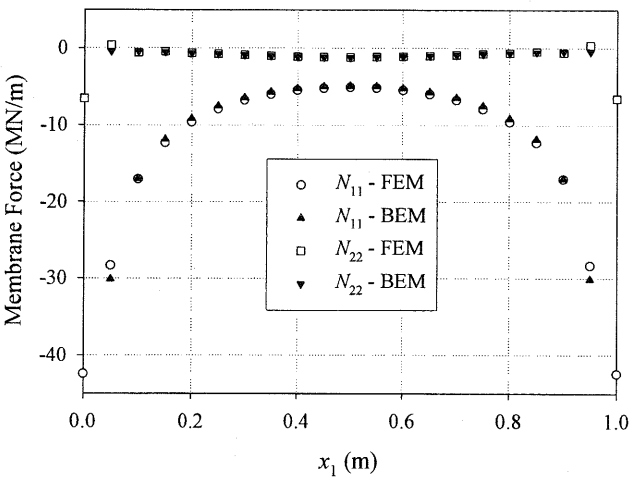

Fig. 10. Membrane forces along the centreline parallel to x_1 axis for the problem of Fig. 7(b).

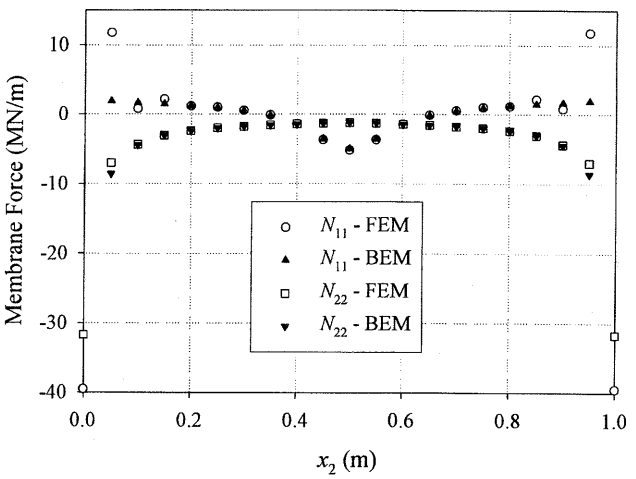

Fig. 11. Membrane forces along the centreline parallel to x_2 axis for the problem of Fig. 7(b).

of 120 elements (50 along each longer and 10 along each shorter side). The FEM analysis of the same plate was performed with a regular mesh of 400 8-node quadrilateral elements (PLANE82) and symmetry accounted for, that is, with only one half of the plate modelled. The predictions of both analyses for the variation of N_{11} and N_{22} along the x_2-axis are shown in Fig. 12. Excellent agreement is noted in this case as well.

All BEM results shown in Figs. 8–12 were obtained using the boundary integral equation for the domain values of the membrane forces, they do not therefore include boundary values. Such values can however be directly obtained by recalling that strain ε_s is determined as a boundary variable according to Eq. (45) and N_n, N_{ns} are known from the boundary conditions. It is thus possible to find N_s, as well as ε_n and ε_{ns} relative to a local $n-s$ frame of reference using constitutive Eq. (1).

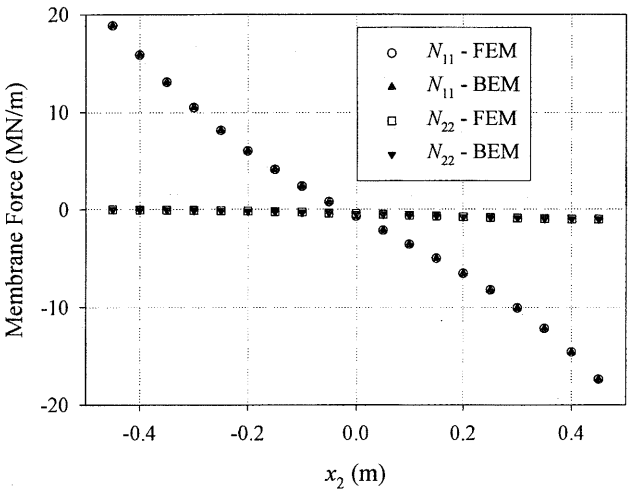

Fig. 12. Membrane forces along x_2 axis for the problem of Fig. 7(c).

9. Conclusions

It has been shown through the solution of several benchmark problems that the BEM formulation is effective and accurate for both flexure and plane stress analysis of laminate plates modelled as elastic and anisotropic. The transition to higher-order boundary elements proved to be advantageous, especially in the case of the extensional problem. Performance improvement was also observed when analytical replaced numerical integration over elements containing the source point. Numerical integration was made more efficient through an adaptive scheme whereby the number of Gaussian quadrature points depended on the proximity of the source point to the element over which the integration was performed. Internal bending moment and membrane force distributions were found in excellent agreement with respective results from exact or finite element analyses. The importance of representing the smoothness of a curvilinear boundary through curvilinear elements was noted. Inaccuracies arising from the use of straight elements may be corrected by accounting for corners, that is, including the contribution of the jump term.

For plates under bending with regular shapes and loading distributions, accurate results are obtained with a relatively small number of elements. An important next step is to test the algorithm and the developed computer codes on problems with greater material and geometric complexity. It is also necessary to validate the membrane analysis on problems with mixed boundary conditions. Established dual reciprocity schemes can be adopted to transform domain integrals to boundary ones. A major challenge in future work would be to explore the possibility of extending the BEM formulation to the analysis of the coupled bending-stretching model for a general laminated plate.

Appendix A

The fundamental solutions (39) and (41) are substituted into Eqs. (23)–(26) to give the kernels

$$\theta_n(u_1^*) = -G_1^{(3)} = \frac{1}{4\pi C_{2222}} \times \mathrm{Re}\left[\sum_{\kappa=1}^{2} \frac{\nu_\kappa}{\beta_\kappa}(2\ln\nu_\kappa + 1)(n_1 + \lambda_\kappa n_2)\right]$$

$$M_n^C(u_1^*) = G_1^{(2)} = -\frac{1}{4\pi C_{2222}} \times \mathrm{Re}\left[\sum_{\kappa=1}^{2} \frac{1}{\beta_\kappa}(2\ln\nu_\kappa + 3)(f_{11} + 2\lambda_\kappa f_{12} + \lambda_\kappa^2 f_{22})\right]$$

$$M_{ns}^C(u_1^*) = -\frac{1}{4\pi C_{2222}} \times \mathrm{Re}\left[\sum_{\kappa=1}^{2} \frac{1}{\beta_\kappa}(2\ln\nu_\kappa + 3)(g_{11} + 2\lambda_\kappa g_{12} + \lambda_\kappa^2 g_{22})\right]$$

$$V_n^C(u_1^*) = -G_1^{(1)} = -\frac{1}{2\pi C_{2222}} \times Re\left[\sum_{\kappa=1}^{2} \frac{1}{\beta_\kappa \nu_\kappa}(h_{111} + \lambda_\kappa h_{112} + \lambda_\kappa^2 h_{122} + \lambda_\kappa^3 h_{222})\right] - \frac{1}{4\pi R C_{2222}} \mathrm{Re}\left[\sum_{\kappa=1}^{2} \frac{1}{\beta_\kappa}(2\ln\nu_\kappa + 3)(f'_{11} + 2\lambda_\kappa f'_{12} + \lambda_\kappa^2 f'_{22})\right]$$

$$\theta_n(u_2^*) = -G_2^{(3)} = -\frac{1}{4\pi C_{2222}} \times \mathrm{Re}\left[\sum_{\kappa=1}^{2} \frac{1}{\beta_\kappa}(2\ln\nu_\kappa + 3)(n_1 + \lambda_\kappa n_2)(m_1 + \lambda_\kappa m_2)\right]$$

$$M_n^C(u_2^*) = G_2^{(2)} = \frac{1}{2\pi C_{2222}} \times \mathrm{Re}\left[\sum_{\kappa=1}^{2} \frac{1}{\beta_\kappa \nu_\kappa}(f_{11} + 2\lambda_\kappa f_{12} + \lambda_\kappa^2 f_{22})(m_1 + \lambda_\kappa m_2)\right]$$

$$M_{ns}^C(u_2^*) = \frac{1}{2\pi C_{2222}} \times \mathrm{Re}\left[\sum_{\kappa=1}^{2} \frac{1}{\beta_\kappa \nu_\kappa}(g_{11} + 2\lambda_\kappa g_{12} + \lambda_\kappa^2 g_{22})(m_1 + \lambda_\kappa m_2)\right]$$

$$V_n^C(u_2^*) = -G_2^{(1)} = -\frac{1}{2\pi C_{2222}} \mathrm{Re}\left[\sum_{\kappa=1}^{2} \frac{1}{\beta_\kappa \nu_\kappa^2}(h_{111} + \lambda_\kappa h_{112} + \lambda_\kappa^2 h_{122} + \lambda_\kappa^3 h_{222})(m_1 + \lambda_\kappa m_2)\right] + \frac{1}{2\pi R C_{2222}} \times \mathrm{Re}\left[\sum_{\kappa=1}^{2} \frac{1}{\beta_\kappa \nu_\kappa}(f'_{11} + 2\lambda_\kappa f'_{12} + \lambda_\kappa^2 f'_{22})(m_1 + \lambda_\kappa m_2)\right]$$

where R is the radius of curvature of the boundary contour and

$$f_{11} = n_\gamma n_\delta C_{11\gamma\delta}, \quad g_{11} = n_\gamma s_\delta C_{11\gamma\delta}, \quad f'_{11} = s_\gamma s_\delta C_{11\gamma\delta},$$

$$f_{12} = n_\gamma n_\delta C_{12\gamma\delta}, \quad g_{12} = n_\gamma s_\delta C_{12\gamma\delta}, \quad f'_{12} = s_\gamma s_\delta C_{12\gamma\delta},$$

$$f_{22} = n_\gamma n_\delta C_{22\gamma\delta}, \quad g_{22} = n_\gamma s_\delta C_{11\gamma\delta}, \quad f'_{22} = s_\gamma s_\delta C_{22\gamma\delta},$$

$$h_{111} = (C_{111\delta} + C_{11\gamma\delta} s_1 s_\gamma) n_\delta,$$

$$h_{112} = [C_{112} + 2C_{121\delta} + (C_{11\gamma\delta} s_2 + 2C_{12\gamma\delta} s_1) s_\gamma] n_\delta,$$

$$h_{122} = [2C_{122\delta} + 2C_{222\delta} + (2C_{12\gamma\delta} s_2 + 2C_{22\gamma\delta} s_1) s_\gamma] n_\delta,$$

$$h_{222} = (C_{222\delta} + C_{22\gamma\delta} s_2 s_\gamma) n_\delta$$

The second derivatives of the first fundamental solution appear in the integral equations yielding internal forces and bending moments. They are obtained as

$$u^*_{1,\alpha\beta}=\frac{1}{4\pi C_{2222}}\mathrm{Re}\left[\sum_{\kappa=1}^{2}\frac{1}{\beta_\kappa}(2\ln v_\kappa+3)e_{\alpha\beta}\right] \tag{A.1}$$

where

$$e_{\alpha\beta}=(\delta_{1\alpha}+\lambda_\kappa\delta_{2\alpha})(\delta_{1\beta}+\lambda_\kappa\delta_{2\beta})$$

The remaining kernels in these integral equations are obtained by substituting Eq. (A.1) into Eqs. (23)–(26). This gives the expressions

$$\theta_n(u^*_{1,\alpha\beta})=\frac{1}{2\pi C_{2222}}\mathrm{Re}\left[\sum_{\kappa=1}^{2}\frac{1}{\beta_\kappa v_\kappa}(n_1+\lambda_\kappa n_2)e_{\alpha\beta}\right]$$

$$M^C_n(u^*_{1,\alpha\beta})=\frac{1}{2\pi C_{2222}}\mathrm{Re}\left[\sum_{\kappa=1}^{2}\frac{1}{\beta_\kappa v^2_\kappa}(f_{11}+2\lambda_\kappa f_{12}+\lambda^2_\kappa f_{22})e_{\alpha\beta}\right]$$

$$M^C_{ns}(u^*_{1,\alpha\beta})=\frac{1}{2\pi C_{2222}}\times\mathrm{Re}\left[\sum_{\kappa=1}^{2}\frac{1}{\beta_\kappa v^2_\kappa}(g_{11}+2\lambda_\kappa g_{12}+\lambda^2_\kappa g_{22})e_{\alpha\beta}\right]$$

$$V^C_n(u^*_{1,\alpha\beta})=-\frac{1}{\pi C_{2222}}\mathrm{Re}\left[\sum_{\kappa=1}^{2}\frac{1}{\beta_\kappa v^3_\kappa}(h_{111}+\lambda_\kappa h_{112}+\lambda^2_\kappa h_{122}+\lambda^3_\kappa h_{222})e_{\alpha\beta}\right]+\frac{1}{2\pi RC_{2222}}\times\mathrm{Re}\left[\sum_{\kappa=1}^{2}\frac{1}{\beta_\kappa v^2_\kappa}(f'_{11}+2\lambda_\kappa f'_{12}+\lambda^2_\kappa f'_{22})e_{\alpha\beta}\right]$$

References

[1] Rizzo FJ, Shippy DJ. A method for stress determination in plane anisotropic elastic bodies. J Compos Mat 1970;4:36–61.

[2] Zastrow U. Solution of plane anisotropic elastostatical boundary-value- problems by singular integral-equations. Acta Mechanica 1982;44:9–71.

[3] Benjumea R, Sikarskie DL. On the solution of plane orthotropic elasticity problems by an integral method. Trans ASME, J Appl Mech 1972;39:801–8.

[4] Vable M, Sikarskie DL. Stress analysis in plane orthotropic material by the boundary element method. Int J Solids Struct 1988;24:1–11.

[5] Lee KJ, Mal AK. A boundary element method for plane anisotropic elastic media. Trans ASME. J Appl Mech 1990;57:600–6.

[6] Wu KC, Chiu YT, Hwu ZH. A new boundary integral-equation formulation for linear elastic solids. J Appl Mech-Trans ASME 1992; 59:344–8.

[7] Wu KC. Nonsingular boundary integral equations for two-dimensional anisotropic elasticity. J Appl Mech-Trans ASME 2000;67: 618–21.

[8] Wu BC, Altiero NJ. A new numerical method for the analysis of anisotropic thin-plate bending problems. Comp Meth Appl Mech Engng 1981;25:343–53.

[9] Irschik H. A boundary-integral equation method for bending of orthotropic plates. Int J Solids Struct 1984;20:245–55.

[10] Kamiya N, Sawaki Y. A general boundary element method for bending analysis of orthotropic elastic plates. Res Mech 1982;5: 329–34.

[11] Shi G, Bezine G. A general boundary integral formulation for the anisotropic plate bending problems. J Compos Mat 1988;22:694–716.

[12] John F. Plane waves and spherical means applied to partial differential equations. New York: Interscience Publishers; 1955.

[13] Syngellakis S, Elzein A. Plate buckling loads by the boundary element method. Int J Num Meth Eng 1994;37:1763–78.

[14] Timoshenko SP, Woinowsky-Krieger S. Theory of plates and shells. New York: McGraw-Hill; 1959.

[15] Lekhnitskii SG. Anisotropic plates. New York: Gordon and Breach; 1968.

[16] ANSYS 6.1, SAS IP Inc., http://www.ansys.com, Canonsburg, PA, 2000.

[17] Whitney JM. Structural analysis of laminated anisotropic plates. Ohio: Technomic Publishing; 1987.